forum acusticum 2026
8-12 September · Graz, Austria

Broadband Noise Attenuation in Ventilated Ducts using an Acoustic Black Hole-Micro-Perforated Panel Structure

Yuchen Zhao[1], Hequn Min[1*], Houcang Tian[2], Ruiyi Zhang[2], Wenxiang Li[1]

[1]*Key Laboratory of Urban and Architectural Heritage Conservation of Ministry of Education, School of Architecture, Southeast University, 2 Sipailou, Nanjing, China*
[2]*China Construction Eighth Engineering Division Corp., Ltd., 1568 Century Avenue, Pudong New Area, Shanghai, China*

Abstract

Broadband noise attenuation in ventilated duct systems remains challenging in the low-to-mid frequency range. This study proposes a ventilated acoustic black hole-micro-perforated panel (ABH-MPP) structure that combines axial geometric variation with sidewall micro-perforations to enhance thermoviscous dissipation. A one-dimensional transfer matrix model is developed and validated against finite element simulations and available data from the literature. Results show broadband sound power dissipation and transmission loss without relying on conventional resonant mechanisms. Introducing internal partitions further enhances dissipation by extending thermoviscous losses from the sidewalls to the partition surfaces, leading to stronger distributed attenuation along the propagation path. Time-domain analysis indicates that the MPP does not weaken the intrinsic slow-wave effect of the ABH; instead, it increases the residence time of acoustic energy and promotes sustained dissipation. Parametric studies identify the influence of key geometric parameters and support a mechanism-based design approach. The ventilation capability of the proposed structure is also evaluated under a typical flow condition, demonstrating that a continuous airflow passage can be maintained.

Keywords: *Micro-perforated panel; Acoustic black hole; Thermoviscous dissipation; Broadband noise attenuation*

1. Introduction

In building ventilation systems and industrial ductwork, conventional duct silencers generally rely on porous acoustic liners [1] or locally resonant structures [2] for noise control. However, porous liners often introduce additional flow resistance, while locally resonant silencers typically exhibit a relatively narrow effective frequency range. Therefore, developing ventilated silencers that simultaneously provide broadband noise attenuation and low flow resistance remains an important research objective.

Micro-perforated panel absorbers (MPAs) [3] and acoustic black holes (ABHs) [4] represent two complementary approaches to acoustic attenuation. MPAs dissipate acoustic energy through thermoviscous losses inside submillimeter perforations, whereas ABHs manipulate wave propagation by means of a power-law geometric taper, leading to wave slowing and energy concentration. Since ABHs mainly manipulate wave propagation rather than dissipate acoustic energy, additional damping mechanisms are generally required to achieve efficient broadband sound absorption. Owing to the complementary characteristics of wave manipulation and energy dissipation, ABH-MPP hybrid structures have recently attracted increasing attention and demonstrated promising broadband acoustic performance [5], [6].

Existing studies on ABH-MPP structures have mainly focused on sound absorption enhancement and structural optimization. Most reported configurations target sound absorption rather than ventilated noise control. Studies on open-ended ABH-MPP structures for ventilated duct applications remain limited. Their acoustic performance and the influence of key design parameters under continuous ventilation conditions have not yet been systematically investigated.

To address these issues, this study proposes a ventilated ABH-MPP duct structure and develops a one-dimensional transfer matrix model. The model is validated against finite element simulations and experimental data available in literature. Based on the validated model, this study further evaluates the acoustic performance, the effects of key design

***Corresponding author**: *hqmin@seu.edu.cn.*

parameters, and the ventilation capability of the proposed structure. The present work extends the application of ABH-MPP structures from sound absorbers to ventilated duct silencers and provides a practical design approach for broadband noise attenuation under ventilated conditions.

2. Modeling

2.1 Finite element model

Fig. 1 shows the configuration of the proposed ABH-MPP structure for ventilated ducts. It consists of an ABH tapered main channel, micro-perforated sidewalls, and a backing cavity divided into multiple sub-cavities by axial partitions (the number of rings is denoted by N). The cross-sectional profile of the ABH channel follows a power-law function given by

$$R(x) = (R_{in} - R_{end})(x/L)^m + R_{end} \quad (1)$$

where R_{in} and R_{end} are the inlet and outlet half-heights of the ABH main channel, respectively, L is the channel length, and m is the power-law exponent.

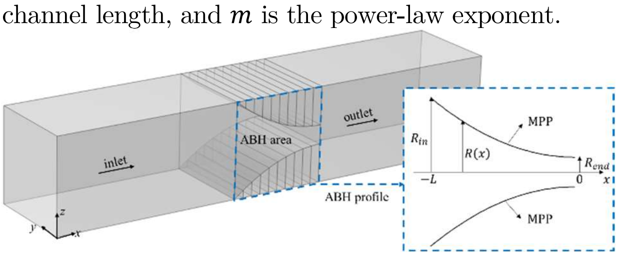

Figure 1. Geometry of the proposed ABH-MPP structure.

The geometry of the ABH-MPP structure is generated according to the power-law profile defined by Eq. (1), with straight duct extensions added at both ends to form the computational domain. A finite element model (FEM) is established in COMSOL Multiphysics using the Thermoviscous Acoustics, Frequency Domain interface. Port boundaries are assigned to the inlet and outlet to define plane-wave excitation and calculate the reflection and transmission coefficients, from which the sound absorption coefficient and transmission loss are obtained. The micro-perforated panel is represented by an equivalent impedance boundary condition based on Maa's theory [3], with its acoustic impedance expressed as

$$Z_{MPP} = Z_{resist} + \mathrm{j} \times Z_{react} \quad (2)$$

$$Z_{resist} = \frac{32\mu t}{\sigma \rho_0 c_0 d^2}\left[\left(1 + \frac{k^2}{32}\right)^{\frac{1}{2}} + \frac{\sqrt{2}}{32} k \frac{d}{t}\right] \quad (3)$$

$$Z_{react} = \frac{\omega t}{\sigma c_0}\left[1 + \left(9 + \frac{k^2}{2}\right)^{-1/2} + 0.85\frac{d}{t}\right] \quad (4)$$

where d is the aperture diameter, t is the panel thickness, and σ is the perforation ratio of the MPP. k is the dimensionless perforation parameter.

2.2 Transfer matrix method

The acoustic response of the proposed structure is predicted using a one-dimensional transfer matrix model (TMM), which is well suited for cascaded duct systems [5]. Under the plane-wave assumption, the ABH channel is discretized into M elements along the axial direction, where each element consists of a tapered main duct coupled to a backing cavity through a micro-perforated boundary.

Within each element, acoustic pressure and volume velocity are related by the transfer matrix of the duct segment, while the coupling through the micro-perforated panel is incorporated using Maa's equivalent impedance model. By enforcing continuity of acoustic pressure p_i and conservation of volume velocity u_i at each interface, the transfer matrix of the i-th element can be expressed as

$$\begin{bmatrix} p_i \\ u_i \end{bmatrix} = T_i \begin{bmatrix} p_{i+1} \\ u_{i+1} \end{bmatrix} = \begin{bmatrix} \cos k_0 d & j\dfrac{\rho_0 c_0}{S_{i+1}} \sin k_0 d \\ j\dfrac{S_i}{\rho_0 c_0} \sin k_0 d & \cos k_0 d \end{bmatrix} \begin{bmatrix} 1 & 0 \\ \dfrac{S_{MPPi}}{Z_{ci} + Z_{MPP}} & 1 \end{bmatrix} \begin{bmatrix} p_{i+1} \\ u_{i+1} \end{bmatrix} \quad (5)$$

where Z_{ci} and Z_{MPP} denote the acoustic impedance of the backing cavity and the intrinsic impedance of the micro-perforated panel, respectively, and S_{MPPi} is the total curved surface area of the micro-perforated sidewalls within the i-th element.

The overall transfer matrix of the ABH-MPP structure is obtained by cascading the transfer matrices of all elements,

$$\begin{bmatrix} p_1 \\ u_1 \end{bmatrix} = T_1 T_2 \cdots \cdots T_M \begin{bmatrix} p_{M+1} \\ u_{M+1} \end{bmatrix} = \begin{bmatrix} T_{11} & T_{12} \\ T_{21} & T_{22} \end{bmatrix} \begin{bmatrix} p_{M+1} \\ u_{M+1} \end{bmatrix} \quad (6)$$

from which the reflection coefficient, transmission coefficient, sound dissipation coefficient, and transmission loss are readily calculated:

$$\eta = 1 - \left(\frac{S_0/\rho_0 c_0 T_{11} - T_{21}}{T_{21} + S_0/\rho_0 c_0 T_{11}}\right)^2 \quad (7)$$

The above formulation corresponds to a rigid termination with the boundary condition u_{M+1}=0. For an open termination, the outlet boundary condition is replaced by $u_{M+1} = p_{M+1} S_0 \ / \ \rho_0 c_0$, and the corresponding transfer matrix is solved accordingly.

3. Results and discussion

Before the subsequent analyses, the proposed finite element model (FEM) and transfer matrix model (TMM) are first validated in Fig.2. Fig. 2(a) compares the predictions obtained by the two methods. The sound power dissipation coefficient and transmission loss agree well over 50-2000Hz, with the peak and valley frequencies showing good consistency. The TMM results exhibit a slight frequency shift of approximately 50 Hz toward higher frequencies, while the maximum difference in transmission loss is about 2 dB, demonstrating the accuracy of the proposed TMM.

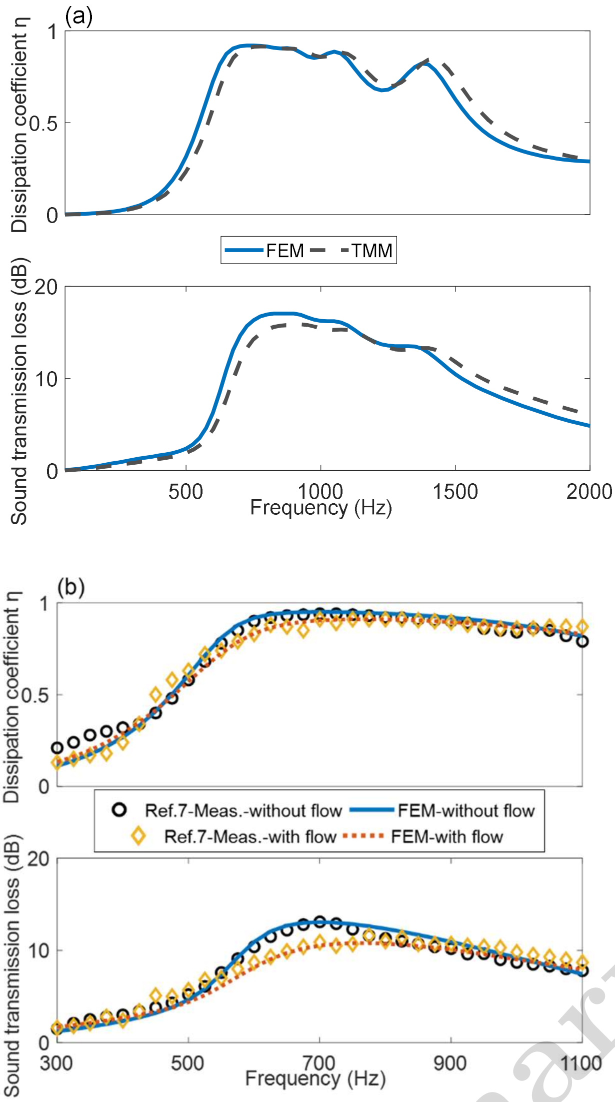

Figure 2. Validation of the numerical and theoretical models for predicting the sound absorption coefficient and transmission loss. (a) Comparison between the FEM and TMM results for the baseline numerical model used throughout this study (L =100 mm, R_{in}=50 mm, R_{end}=10 mm, m=2; MPP parameters: t=d=0.8 mm and σ=1%). (b) Comparison between the FEM results and the experimental data reported in Ref. [7] under no-flow and 30 m/s airflow conditions.

Fig. 2(b) further compares the FEM predictions with the experimental results reported in Ref. [7] under no-flow and 30 m/s airflow conditions. Good agreement is achieved for both the dissipation coefficient and the transmission loss in both cases, confirming the reliability of the proposed FEM. It is also observed that even at an airflow velocity of 30 m/s, the influence of airflow on the sound power dissipation coefficient is negligible, while the reduction in transmission loss remains below 3 dB. Since 30 m/s is higher than the operating velocity in most ventilation duct systems, the subsequent analyses are performed under no-flow conditions to improve computational efficiency.

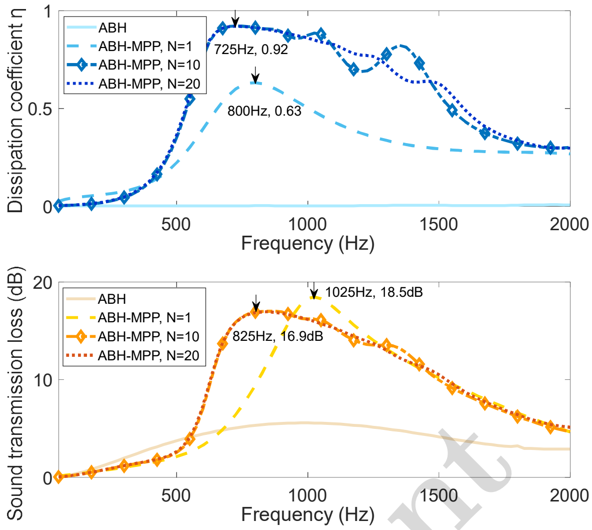

Figure 3. Effect of introducing the MPP and increasing the number of rings on the sound power dissipation coefficient and transmission loss.

Fig. 3 compares the acoustic performance of the conventional ABH structure and the proposed ABH-MPP structure with different numbers of rings. The conventional ABH exhibits negligible sound power dissipation, and its transmission loss remains below 10 dB over the frequency range of 50-2000 Hz. After introducing the micro-perforated panel, both the dissipation coefficient and the transmission loss are significantly enhanced. For the ABH-MPP structure with N=1, a dissipation peak of 0.63 is obtained at 800 Hz, while the transmission loss reaches 18.5 dB at 1025 Hz. As the number of rings increases to N=10 and 20, the dissipation bandwidth is further broadened, with the peak dissipation coefficient increasing to approximately 0.92 at 725 Hz. Meanwhile, the transmission loss peak shifts to a lower frequency of 825 Hz with a value of 16.9 dB, indicating an enhanced low-frequency attenuation capability. It is also observed that the acoustic responses for N=10 and 20 almost completely overlap, suggesting that the acoustic performance gradually converges as the number of rings increases.

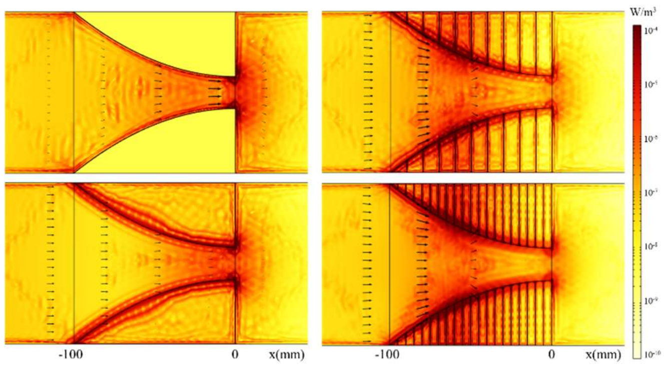

Figure 4. Distributions of total thermoviscous loss and acoustic intensity vectors at 800 Hz for the ABH, ABH-

MPP (N=1), ABH-MPP (N=10), and ABH-MPP (N=20) structures.

To further reveal the mechanism responsible for the enhanced broadband acoustic performance, the distributions of the total thermoviscous loss and acoustic intensity vectors at 800 Hz are compared for the four structures. As shown in Fig. 4, acoustic energy in all cases propagates toward and gradually concentrates near the tapered end of the ABH, indicating that neither the introduction of the MPP nor the increase in the number of rings alters the fundamental wave-guiding behavior of the ABH. However, after introducing the MPP, the acoustic intensity vectors are clearly deflected toward the micro-perforated sidewalls and guided into the backing cavities, indicating that more acoustic energy enters the dissipative regions. Correspondingly, the thermoviscous loss, which is weak and mainly confined to the boundary layer in the conventional ABH, becomes concentrated around the MPP surfaces. As the number of rings further increases, the partition walls provide additional thermoviscous boundary layers, extending the dissipation regions throughout the sub-cavities and promoting more distributed acoustic energy dissipation. Consequently, the residual acoustic intensity near the outlet is significantly reduced for all ABH-MPP structures, indicating that more acoustic energy is dissipated before leaving the duct. These observations are consistent with the substantially improved sound power dissipation coefficient and transmission loss at around 800 Hz shown in Fig. 3.

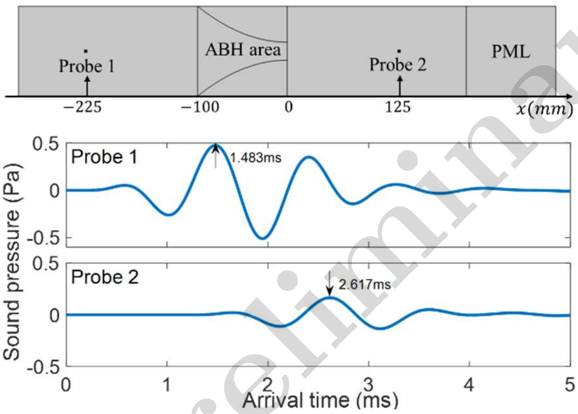

Figure 5. Time-domain simulation for evaluating the slow-wave effect in the ABH-MPP structure. Two pressure probes are used to determine the propagation velocity from the arrival time difference of the pressure peaks.

To further investigate whether the slow-wave effect is preserved in the proposed ABH–MPP structure with a practical truncated end radius of 10 mm, the time-domain approach illustrated in Fig. 5 is adopted. Two pressure probes are placed at x =−225 mm and x =125 mm, and the average propagation velocity is determined from the arrival time difference of the pressure peaks. For the ABH-MPP structure with N=1, the measured time delay is 1.134 ms, corresponding to an average propagation velocity of 309 m/s over a propagation distance of 350 mm. In comparison, the conventional ABH exhibits an average propagation velocity of 333 m/s, indicating that introducing the MPP does not weaken the intrinsic slow-wave effect of the ABH. When the number of rings is further increased to N=10 and 20, the average propagation velocity is approximately 318 m/s in both cases, showing only a minor variation compared with the N=1 configuration. However, as shown in Fig. 3, the dissipation coefficient and transmission loss continue to improve significantly with increasing N. These results suggest that the enhanced broadband acoustic performance is not primarily associated with a stronger slow-wave effect, but is mainly attributed to the increased distributed thermoviscous dissipation introduced by the MPP and the partitioned sub-cavities.

Owing to the limited length of this conference paper, only two representative design parameters are discussed. The outlet half-height R_{end} and the perforation ratio σ are selected as representative design variables for the ABH geometry and the MPP, respectively. Fig. 6 illustrates their influence on the acoustic performance of the proposed structure.

As shown in Fig. 6(a), increasing R_{end} shifts the dissipation coefficient toward higher frequencies by approximately 100 Hz, while the overall curve shape remains nearly unchanged, indicating that the truncated end height mainly affects the operating frequency rather than the overall dissipation characteristics. Meanwhile, the transmission loss decreases over the entire frequency range, with the average value dropping by more than 5 dB over 50-2000 Hz. This can be attributed to the larger truncated end, which provides a less constricted propagation path for sound transmission.

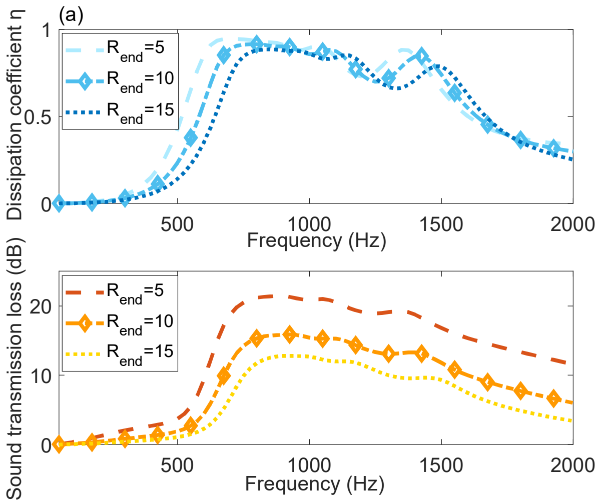

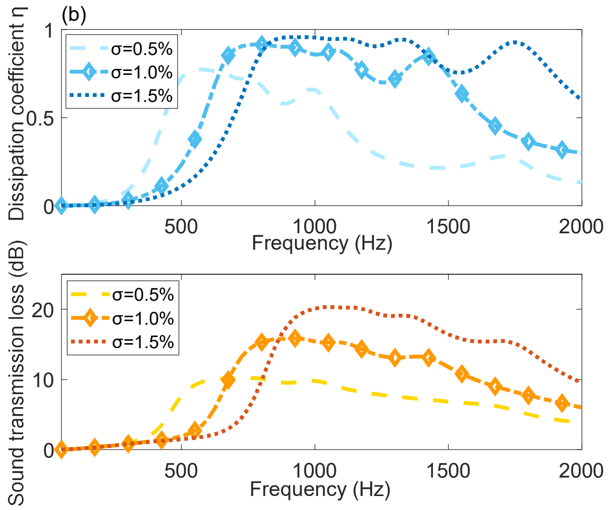

Figure 6. Effects of two representative design parameters on the acoustic performance of the proposed ABH-MPP structure (N =10): (a) outlet half-height R_{end} ; (b) perforation ratio σ.

Fig. 6(b) shows that increasing the perforation ratio shifts both the dissipation coefficient and the transmission loss toward higher frequencies. Meanwhile, the effective dissipation bandwidth is broadened, and the average transmission loss over 50-2000 Hz increases by more than 5 dB. These results demonstrate that the proposed analytical model can effectively capture the influence of key design parameters and provide a useful basis for future parameter optimization and practical duct silencer design.

Fig. 7 presents the velocity distribution and streamlines of the proposed ABH-MPP structure (N=10) at a Mach number of 0.05 to evaluate its ventilation capability. In the present model, the micro-perforations are not explicitly modeled, and only the primary ventilation channel is considered. Since the perforations are much smaller than the main duct, their influence on the overall airflow path is negligible; therefore, the local flow effects and acoustic impedance associated with the micro-perforations are beyond the scope of the present aerodynamic analysis.

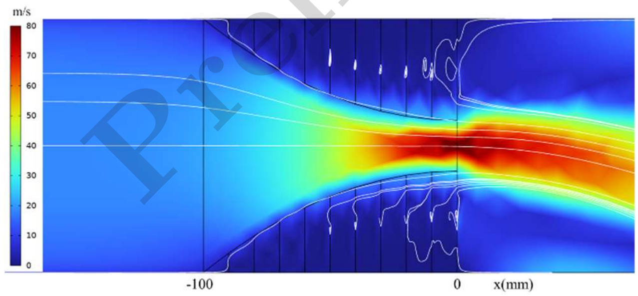

Figure 7. Airflow velocity distribution and streamlines in the proposed ABH-MPP structure under a typical ventilation condition (Mach number = 0.05).

As shown in Fig. 7, the airflow accelerates smoothly through the tapered ABH section owing to the gradually decreasing cross-sectional area. The streamlines remain continuous throughout the main channel and pass smoothly through the tapered region, indicating that the proposed structure maintains a continuous and stable ventilation path. Although limited local recirculation is observed in the wake of several ribs, no obvious large-scale flow separation or recirculation occurs. After passing through the tapered section, the flow gradually redistributes in the downstream straight duct. Overall, the ABH geometry and the internal ribs do not significantly obstruct the main airflow, demonstrating that the proposed structure can maintain good ventilation while incorporating acoustic attenuation components.

4. Conclusions

This paper proposes an acoustic black hole with micro-perforated sidewalls for broadband noise attenuation under ventilated conditions. Unlike conventional ABH absorbers, the proposed structure adopts an open-ended configuration with a relatively large truncated end, providing a continuous airflow passage while improving its practical applicability for duct silencers. Despite these engineering-oriented modifications, the proposed structure preserves the beneficial wave-guiding characteristics of the ABH. The introduction of the micro-perforated sidewalls further enhances both the sound power dissipation and the transmission loss, while increasing the number of partition rings broadens the effective attenuation bandwidth. Time-domain analysis shows that the slow-wave effect remains in the proposed structure but changes only slightly with increasing ring number, suggesting that the enhanced broadband performance is mainly associated with the distributed thermoviscous dissipation introduced by the MPP and the partitioned sub-cavities rather than with a further enhancement of the slow-wave effect. Parametric studies further identify the influences of the truncated end height and perforation ratio on the acoustic performance, providing useful guidance for practical design. Flow simulations demonstrate that the proposed structure maintains a continuous ventilation path with only limited local flow disturbance. Future work will incorporate acoustic–flow coupling and experimental investigations under practical operating conditions to further improve the model and support engineering applications.

5. Acknowledgments

This work is supported by the Natural Science Foundation of China (Grant No. 51408113), the Natural Science Foundation of Jiangsu Province, China (Grant No. BK20140632), and the research project "Key Technology Research and Application of Acoustic Engineering Construction for International Top-tier Concert Halls" commissioned by China Construction Eighth Engineering Division Corp., Ltd. (Project No. 013042024011003036).

References

[1] X. Song, H. J. Yang, X. X. Xu, J. K. Xu, D. Sui, T. F. Zhao, and J. Zhou: “Flow duct noise attenuation with micro-scale optimization of porous liner,” International Journal of Mechanical Sciences, vol. 297, no. 110373, 2025.

[2] X. C. Zhao, G. M. Liu, C. M. Zhao, and K. Grosh: “Broadband noise attenuation using a variable locally reacting impedance,” Journal of the Acoustical Society of America, vol. 141, no. 1, pp. 147-158, 2017.

[3] D. Y. Maa: “Theory and design of sound absorption structure of micro-perforated plate,” Scientia Sinica, vol. 18, no. 1, pp. 55-71, 1975.

[4] M. A. Mironov: “Propagation of a flexural wave in a plate whose thickness decreases smoothly to zero in a finite interval,” Soviet Physics Acoustics, vol. 34, no. 3, pp. 318-319, 1988.

[5] X. Yu, Y. Z. Mi, W. Zhai, and L. Cheng: “Principles of progressive slow-sound and critical coupling condition in broadband sonic black hole absorber,” Journal of the Acoustical Society of America, vol. 154, no. 5, pp. 2988-3003, 2023.

[6] S. H. Li, X. Yu, and L. Cheng: “Enhancing wave retarding and sound absorption performances in perforation-modulated sonic black hole structures,” Journal of Sound and Vibration, vol. 596, no. 118765, 2025.

[7] C. Maury, T. Bravo, and F. Ali: "Micro-perforated rainbow-trapping silencers with broadband sound dissipation and reduced drag under low-speed grazing flow," Journal of Sound and Vibration, vol. 616, no. 119228, 2025.